

## RESEARCH ARTICLE

10.1002/2015JA022071

## Key Points:

- The FAC in the PSBLs studied by both *M* field and its carriers in a substorm time
- The species type and energy range of the FAC carriers are identified for the first time
- Not only electrons but also ions can be significant to carry the FACs in the magnetotail

## Correspondence to:

Z. W. Cheng,  
zwcheng@spaceweather.ac.cn

## Citation:

Cheng, Z. W., J. C. Zhang, J. K. Shi, L. M. Kistler, M. Dunlop, I. Dandouras, and A. Fazakerley (2016), The particle carriers of field-aligned currents in the Earth's magnetotail during a substorm, *J. Geophys. Res. Space Physics*, 121, 3058–3068, doi:10.1002/2015JA022071.

Received 22 OCT 2015

Accepted 15 MAR 2016

Accepted article online 21 MAR 2016

Published online 9 APR 2016

## The particle carriers of field-aligned currents in the Earth's magnetotail during a substorm

Z. W. Cheng<sup>1,2</sup>, J. C. Zhang<sup>2</sup>, J. K. Shi<sup>1</sup>, L. M. Kistler<sup>2</sup>, M. Dunlop<sup>3,4</sup>, I. Dandouras<sup>5</sup>, and A. Fazakerley<sup>6</sup>

<sup>1</sup>State Key Laboratory of Space Weather, NSSC/CAS, Beijing, China, <sup>2</sup>Space Science Center, University of New Hampshire, Durham, New Hampshire, USA, <sup>3</sup>Space Science Institute, School of Astronautics, Beihang University, Beijing, China, <sup>4</sup>SSTD, Rutherford Appleton Laboratory, Didcot, Oxfordshire, UK, <sup>5</sup>University of Toulouse, UPS, IRAP, and CNRS, Toulouse, France, <sup>6</sup>MSSL, University College London, London, UK

**Abstract** Although the particle carriers of field-aligned currents (FACs) in the Earth's magnetotail play an important role in the transfer of momentum and energy between the solar wind, magnetosphere, and ionosphere, the characteristics of the FAC carriers have been poorly understood. Taking advantage of multiinstrument magnetic field and plasma data collected by the four spacecraft of the Cluster constellation as they traversed the northern plasma sheet boundary layer in the magnetotail on 14 September 2004, we identified the species type and energy range of the FAC carriers for the first time. The results indicate that part of tailward FACs is carried by energetic keV ions, which are probably originated from the ionosphere through outflow, and they are not too small ( $\sim 2$  nA/m<sup>2</sup>) to be ignored. The earthward (tailward) FACs are mainly carried by the dominant tailward (earthward) motion of electrons, and higher-energy electrons (from  $\sim 0.5$  to 26 keV) are the main carriers.

### 1. Introduction

Field-aligned currents (FACs), also called the Birkeland currents, flow into and out of the ionosphere along magnetic field lines. They were first detected by satellite in the 1960s [Zmuda *et al.*, 1966; Cummings and Dessler, 1967] and have been observed in the different regions of the geospace system. In the ionosphere, Iijima and Potemra [1976, 1978] have determined the large-scale characteristics of the FACs—the region 1 (R1) and region 2 (R2) current systems—by using magnetic field data. In the magnetotail, the presence of FACs has been confirmed with both magnetic field [Aubry *et al.*, 1972; Ueno *et al.*, 2002; Shi *et al.*, 2010] and plasma measurements [Frank, 1981; Eriksson *et al.*, 2002; Wright *et al.*, 2008].

Knowledge of the FAC carriers and their dynamics is important for the understanding of the energy transfer between the solar wind, magnetosphere, and ionosphere. It is also crucial for the understanding of some of the dominant aurora physical processes occurring in the polar region. In early studies, it is found that at low altitudes, the visual aurora is associated with upward flowing FAC which is mainly carried by precipitating electrons in the energy range of about 0.5 keV to tens of keV [Cassery and Cloutier, 1975; Berko *et al.*, 1975; McDiarmid *et al.*, 1978]. Electrons are believed to be the main carriers of both upward and downward FACs in the polar region because currents carried by these electrons were found to be comparable to currents derived from simultaneous magnetic field measurements [Torbert and Carlson, 1980; Morooka *et al.*, 1998].

However, limited investigation has focused on the carriers of FACs in the plasma sheet boundary layer (PSBL) in the magnetotail [Frank *et al.*, 1981]. Because the FAC densities in the magnetotail are less than those at low altitudes by almost 2 or 3 orders of magnitudes, it is difficult to directly derive FACs from plasma measurements. Shi *et al.* [2014] deduced that the field-aligned electrons were the main contributors to FACs in a high-flux electron disturbance in the magnetotail, but the exact carriers of the FACs have not been definitively identified.

Both electrons and ions can move in geospace along the magnetic field lines. FACs are the sum of the currents carried by these charged particle species. It is generally believed that the electrons were the main carriers of upward and downward FACs in the aurora region. However, studies showed that the large-scale FACs are sometimes determined by ions, especially in the cusp [Yamauchi *et al.*, 1998]. Other studies have shown that an increase in ionospheric ion outflow can be associated with increases in FAC [Winglee *et al.*, 2005] and upward FAC can drive O<sup>+</sup> upwellings [Gombosi and Nagy, 1989]. Ion outflows are generated during heating of the ionosphere as a result of the precipitation of accelerated electrons during substorms. Ion

heating by FAC-driven instabilities can cause ion outflows in the high-latitude ionosphere [Strangeway *et al.*, 2000; Zheng *et al.*, 2005; Moore *et al.*, 2014; Welling *et al.*, 2015]. Simulation results show that the upward ions originally from the nightside auroral oval will drift into the center plasma sheet along the magnetic field lines in the plasma sheet boundary and have an important effect on the FACs [Zhang *et al.*, 2007]. Without measurements of ion composition in a full energy range, the FAC densities cannot be calculated accurately. FACs are usually estimated with magnetic field data. Before the Cluster mission, FACs in the magnetotail had been studied with magnetic field measurements acquired by one or two satellites, and the current density could only be roughly estimated [Eastman *et al.*, 1985; Ohtani *et al.*, 1988; Ueno *et al.*, 2002]. The four Cluster spacecraft make multipoint measurements of magnetic field data [Shi *et al.*, 2010], making it possible to calculate the current density more accurately. Some of the FAC results in the magnetotail showed decent consistency with those at low altitudes [Shi *et al.*, 2010; Cheng *et al.*, 2013]. In this paper, we perform a case study of an FAC event by using in situ magnetic field and plasma measurements from the four Cluster spacecraft to examine the carriers of FACs in the magnetotail during a substorm recovery phase. For the first time, we pinpoint exact particles that carry the FACs and their energy ranges.

## 2. Data and Methods

### 2.1. Data

We use magnetic field data from the Fluxgate Magnetometer (FGM) [Balogh *et al.*, 1997] and electron data from the Plasma Electron And Current Experiment (PEACE) [Johnstone *et al.*, 1997] on board the Cluster spacecraft. Ion data are from the Cluster Hot Ion Analyzer (HIA). HIA is one of the two instruments of the Cluster Ion Spectrometry (CIS) instrument [Rème *et al.*, 2001], and the other CIS instrument is the Composition and Distribution Function (CODIF) analyzer [Möbius *et al.*, 1998]. The corresponding interplanetary magnetic field (IMF) and auroral electrojet (AE), *AU*, and *AL* indices were obtained from the OMNI database. The *AU* and *AL* indices represent the current intensity of the eastward and westward auroral electrojets, respectively. All the four Cluster spacecraft have an apogee of 19.6 Earth radii ( $R_E$ ) and an orbital period of 57 h. From July to October of 2004, they cross the plasma sheet in the magnetotail, and the interspacecraft distance was about 1000 km, which is typically optimal for the calculation of current density using the curlometer method [Dunlop *et al.*, 1988]. In total, each spacecraft has 63 PSBL crossings during the Cluster tail “season.”

### 2.2. Methods

In this study, the PSBL is identified by plasma  $\beta$  (the ratio of plasma pressure to magnetic pressure), which is given by the condition  $0.01 \leq \beta \leq 1$ . The lobe region is given by the condition  $\beta < 0.01$ , and the plasma sheet is given by the condition  $\beta > 1$  [Ueno *et al.*, 2002]. We also examine the magnetic field components  $B_x$ ,  $B_y$ , and  $B_{xy}$  ( $B_{xy} = \sqrt{B_x^2 + B_y^2}$ ) [Ohtani *et al.*, 1988; Shi *et al.*, 2010].

First, the FAC density is calculated with the magnetic field data obtained by the four spacecraft, using the curlometer technique [Dunlop *et al.*, 1988].

This method based on the Ampere’s law is as follows:

$$\vec{J} = \frac{\nabla \times \vec{B}}{\mu_0} \quad (1)$$

where  $\vec{J}$  is the current density and  $\mu_0$  is the magnetic permeability of free space.

The magnetic field curl can be written as

$$\nabla \times \vec{B} = \sum_{\alpha=1}^4 \vec{k}_\alpha \times \vec{B}_\alpha \quad (2)$$

where  $\vec{k}_\alpha$  is a vector constant defined as

$$\vec{k}_\alpha = \frac{\vec{r}_{\beta\gamma} \times \vec{r}_{\beta\lambda}}{\vec{r}_{\beta\alpha} \cdot (\vec{r}_{\beta\gamma} \times \vec{r}_{\beta\lambda})} \quad (3)$$

where  $\vec{r}_{\beta\gamma}$  is the distance between each two spacecraft,  $\vec{r}_{\beta\gamma} = \vec{r}_\gamma - \vec{r}_\beta$  and  $\alpha, \beta, \gamma, \lambda = 1, 2, 3, 4$ , respectively [Chanteur, 1998; Dunlop *et al.*, 2002].

With the calculated current, the FAC can be obtained with the projection of

$$j_{\parallel} = \vec{j} \cdot \vec{B} / |\vec{B}| \quad (4)$$

Because the accuracy of the calculated current density is strongly related to the shape of the tetrahedron and the magnetic configuration, we use  $Q$  to evaluate the data quality of the calculated FAC.  $Q$  is defined as

$$Q = |\nabla \cdot \vec{B}| / |\nabla \times \vec{B}| \quad (5)$$

where

$$\nabla \cdot \vec{B} = \sum_{\alpha=1}^4 \vec{k}_{\alpha} \cdot \vec{B}_{\alpha}$$

In this study, we take  $Q < 0.3$  to ensure the result quality [Shi *et al.*, 2010; Cheng *et al.*, 2013]. The densities of FACs in this study were large enough (more than 4 nA/m<sup>2</sup>). This ensures the current background noise, and the errors resulting from the current calculation using the tetrahedron approximation are low. Typically, the curlometer gave estimates of the FAC density with errors of ~12% in our previous study [Shi *et al.*, 2010]. In this study, during the recovery phase of the substorm, the errors ranged from 6.2% to 16.7% (Figure 1e showed that current is approximately 0.8 nA/m<sup>2</sup>, except for the FAC cases with a density of 4.9–13.0 nA/m<sup>2</sup>). The method gives a reasonable estimate of the current within this accuracy.

Second, the FAC density is calculated with plasma data. When electrons (ions) move at a velocity along the magnetic field line  $\vec{v}_{\parallel e}$  ( $\vec{v}_{\parallel i}$ ), they cause a FAC density  $\vec{j}_{\parallel e} = ne\vec{v}_{\parallel e}$  ( $\vec{j}_{\parallel i} = ne\vec{v}_{\parallel i}$ ), and the total FAC density is  $\vec{j}_{\parallel \text{total}} = ne(\vec{v}_{\parallel i} - \vec{v}_{\parallel e})$  ( $n$  is the number density of the electrons or ions,  $e$  is the unit electric charge,  $\vec{v}_{\parallel i}$  is the ions velocity, and  $\vec{v}_{\parallel e}$  is the electron velocity). There is a high possibility for having large errors with this method. It is difficult to determine the error ranges of the plasma method directly. More accurate current density is usually from the calculation with the curlometer method. Thus, the difference between the two results should be the error with the plasma method.

At last, through comparing the calculation results by the two methods, we find out which particles are the carriers and what their energies are.

### 3. Observations

#### 3.1. The FAC Event

The FAC event was observed during 18:49–19:04 UT on 14 September 2004 in the recovery phase of a substorm. The Cluster moved from (−16.64, 1.59, 1.91) $R_E$  to (−16.76, 1.61, 1.76) $R_E$  in the geocentric solar magnetospheric (GSM) coordinates and crossed the northern PSBL on the duskside. A strong FAC disturbance was detected during that period. Figure 1 shows the event. From top to bottom are the IMF components ( $B_x$ ,  $B_y$ , and  $B_z$ ) (Figure 1a), Cluster observations of magnetic field components ( $B_x$ ,  $B_y$ , and  $B_z$ ) (Figure 1b) and plasma beta (Figure 1c), geomagnetic indices ( $AE$ ,  $AU$ , and  $AL$ ) (Figure 1d), and the FAC densities calculated with the curlometer technique (FAC<sub>B</sub>) (Figure 1e). The two vertical solid red lines indicate the start (18:49 UT) and end (19:04 UT) times of the event. IMF  $B_z$  component kept southward before the substorm onset for more than 1 h, and then IMF  $B_z$  started to increase at about 18:30 UT (marked by a black vertical dotted line) and then turned from southward to northward, shown in Figure 1a. Figure 1d shows that the  $AL$  index started to decrease at the same time and reached the minimum value at −900 nT after about 15 min. At ~18:43 UT (marked by a purple vertical dotted line), Cluster observed magnetic field dipolarization,  $B_z$  reached its peak at about 18:49 UT and kept high value (from about 10 to 20 nT) while  $B_x$  decreased from around 40 to 10 nT, shown in Figure 1b. The plasma beta sharply increased from about 0.001 to 1. It indicates that the Cluster crossed from the lobe region to the PSBL region (much closer to the plasma sheet). From about 18:49 to 19:04 UT, the IMF  $B_x$  and  $B_z$  were mostly positive with a periodic disturbance. The IMF  $B_y$  changed from positive to negative, and its magnitude was less than 5 nT, shown in Figure 1a. The FAC density reached the maximum value (about 13 nA/m<sup>2</sup>, marked by a green vertical dotted line) at ~18:54 UT (Figure 1e). Cheng *et al.* [2007, 2013] found that the most probable value of FAC density in the PSBL region is about

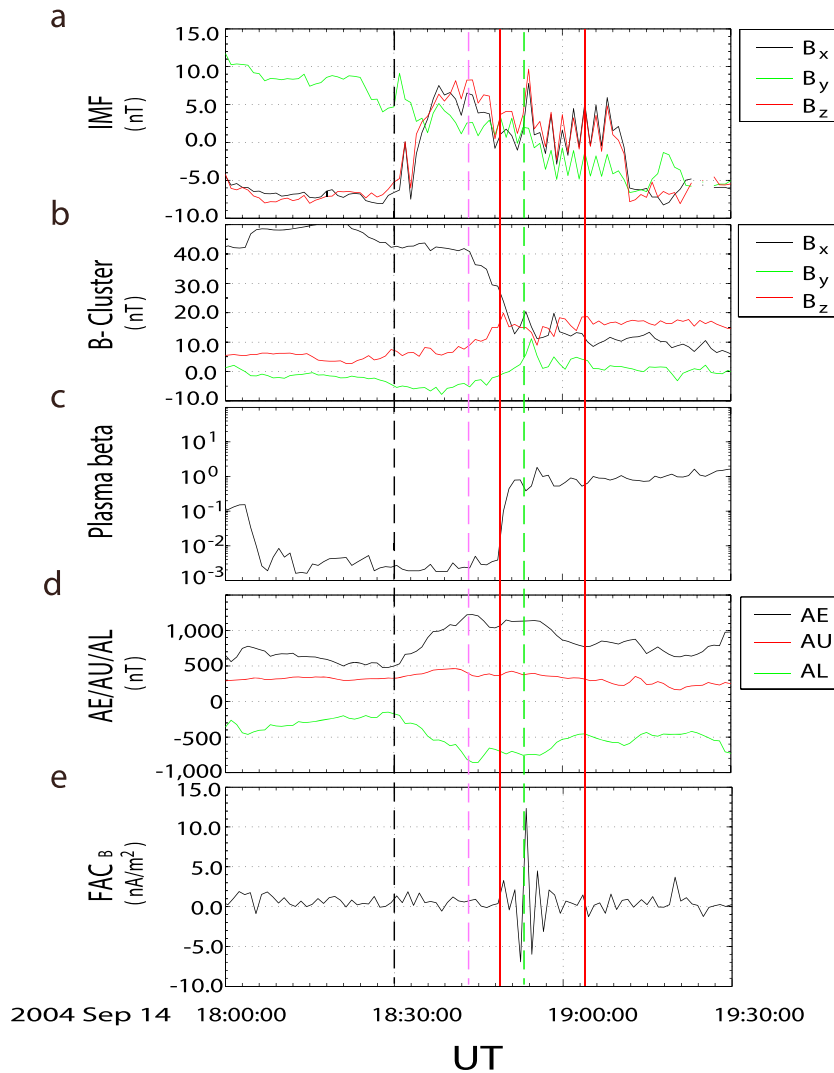


**Figure 1.** The FACs in the magnetotail observed by Cluster on 14 September 2004. (a) The interplanetary magnetic field  $B_x$  (black),  $B_y$  (red), and  $B_z$  (green) components in the GSM coordinates. (b) Magnetic field  $B_x$  (black),  $B_y$  (red), and  $B_z$  (green) components in the magnetotail in the GSM coordinates. (c) Plasma beta from Cluster observations in the magnetotail. (d) Geomagnetic activity indices AE/AU/AL. (e) The FAC densities calculated with the curlometer technique ( $FAC_B$ ). The two vertical red solid lines indicate the start (1849 UT) and end (1904 UT) times of the FAC event.

$3 \text{ nA/m}^2$ , and further study indicated that the average FAC density in the northward PSBL is  $\sim 4.9 \text{ nA/m}^2$ . During a substorm, the large-scale FAC from the magnetotail to the ionosphere exhibited great disturbances, and its density was larger than normal [Chun and Russell, 1991]. Thus, as in the present event, substorms provide a good chance for us to study the carriers of FAC.

From the magnetic field components ( $B_x$ ,  $B_y$ , and  $B_z$ ) [Ohtani et al., 1988; Shi et al., 2010] and plasma beta of Cluster [Ueno et al., 2002], we were able to identify the different regions of the magnetotail. Figure 2 schematically demonstrates the crossing process of the four Cluster spacecraft (C1, C2, C3, and C4) in the midtail. The locations of the four spacecraft indicate the realistic positions while they crossed the PSBL. When the substorm began, the plasma sheet began to thin. The Cluster spacecraft stayed in the lobe region in the growth phase and early expansion phase (from 18:04 to 18:26 UT), and there was no FAC disturbance present. From 18:27 to 18:48 UT, although the plasma sheet began to thicken, the Cluster spacecraft still remained in the lobe region. During the recovery phase, the Cluster spacecraft returned to the PSBL (from about 18:49 to 19:04 UT), and intense FACs were detected. C3 entered the PSBL first and detected the FACs with valid plasma data during the whole crossing process.

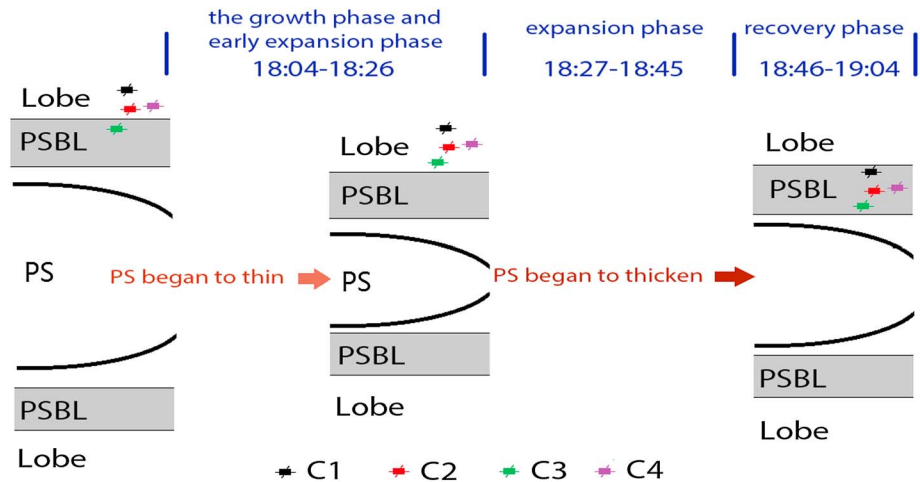


**Figure 2.** A schematic sketch of the Cluster crossing process in the magnetotail during the different phases of the substorm on 14 September 2004. Positions of Cluster spacecraft C1, C2, and C4 relative to C3 indicate that C3 was located in the PSBL before the substorm and returned to the PSBL in the recovery phase (from about 1849 to 1904 UT).

### 3.2. FACs Carried by Ions and Electrons

Figure 3 demonstrates the FAC calculation results using plasma and magnetic field data during the substorm recovery phase. In plasma data, we distinguish the ions and electrons. The ion FAC density versus time, energy versus time flux spectrogram, and pitch angle versus time flux spectrogram in the energy range of 0.005–32 keV are shown in Figures 3a–3c. The color bar denotes the energy flux (eflux). The large tailward FACs and their corresponding ion energy range and pitch angles are marked by the two vertical red lines. The electron FAC density versus time, energy versus time flux spectrogram, and pitch angle versus time flux spectrogram in the energy range of 0.001–26 keV are shown in Figures 3d–3f. The large earthward FACs and their corresponding energy range and pitch angles are marked by the two vertical black lines. The plasma measurements are from the Cluster/CIS and PEACE on board C3. Figure 3g shows the FAC calculation results. The black line is  $FAC_p$ , which denotes the FAC density calculated with C3 plasma data (ions and electrons). The blue line is  $FAC_B$ , which denotes the FAC density calculated with the magnetic field data using the curlometer technique. It is clear that  $FAC_p$  and  $FAC_B$  (for every peak and valley) are very similar to each other. Generally, the current density carried by ions is small (far less than  $1 \text{ nA/m}^2$ ). Compared with electrons, they are often negligible. In this study, we found that the maximum tailward ion FAC was  $\sim 2 \text{ nA/m}^2$  (Figure 3a) while the electron FAC was earthward and its density was  $\sim 4 \text{ nA/m}^2$ . This indicates that the motion directions of ions and electrons are both tailward. In this situation, the ion FAC carriers were a large fraction of the total carriers and could not be ignored. As shown in Figure 3b, the ion fluxes were enhanced above 1 keV during roughly in the same time period as the FAC enhancement. The pitch angle distribution (Figure 3c) indicates that the ion enhancement occurred in directions predominantly antiparallel to the ambient magnetic field, i.e., with  $120^\circ$ – $180^\circ$  pitch angles. Thus, the ion flow directions were tailward, consisted with the directions of the FACs. From Figures 3d–3f, we can see that the FACs are mainly carried by the dominant flow of electrons with higher energies.

### 3.3. Energy Ranges of the FAC Carriers

In order to find out the main energy range that these FAC carriers are in, we examined the pitch angle versus time flux spectrogram in the different energy range. For ions, the results are shown in Figure 4. From top to bottom are the pitch angle versus time flux spectrogram in the energy ranges of 0.005 to 1, 1 to 10, 10 to 32 keV, and the FACs carried by ions (Figures 4a–4d). The large tailward FACs and their corresponding energy ranges are marked by the two vertical black lines. Note that the color scale in Figures 4a is different from Figures 4b and 4c by a factor of 10. Figure 4a shows that in the energy range of 0.005 to 1 keV, there was almost no net antiparallel ion motion. The ion fluxes increased obviously above 1 keV; therefore, the FAC was primarily carried by ions in the energy range of about 1 to 32 keV (Figures 4b and 4c). We distinguished different ion species and calculated the FAC densities carried by  $H^+$  and  $O^+$  using data from

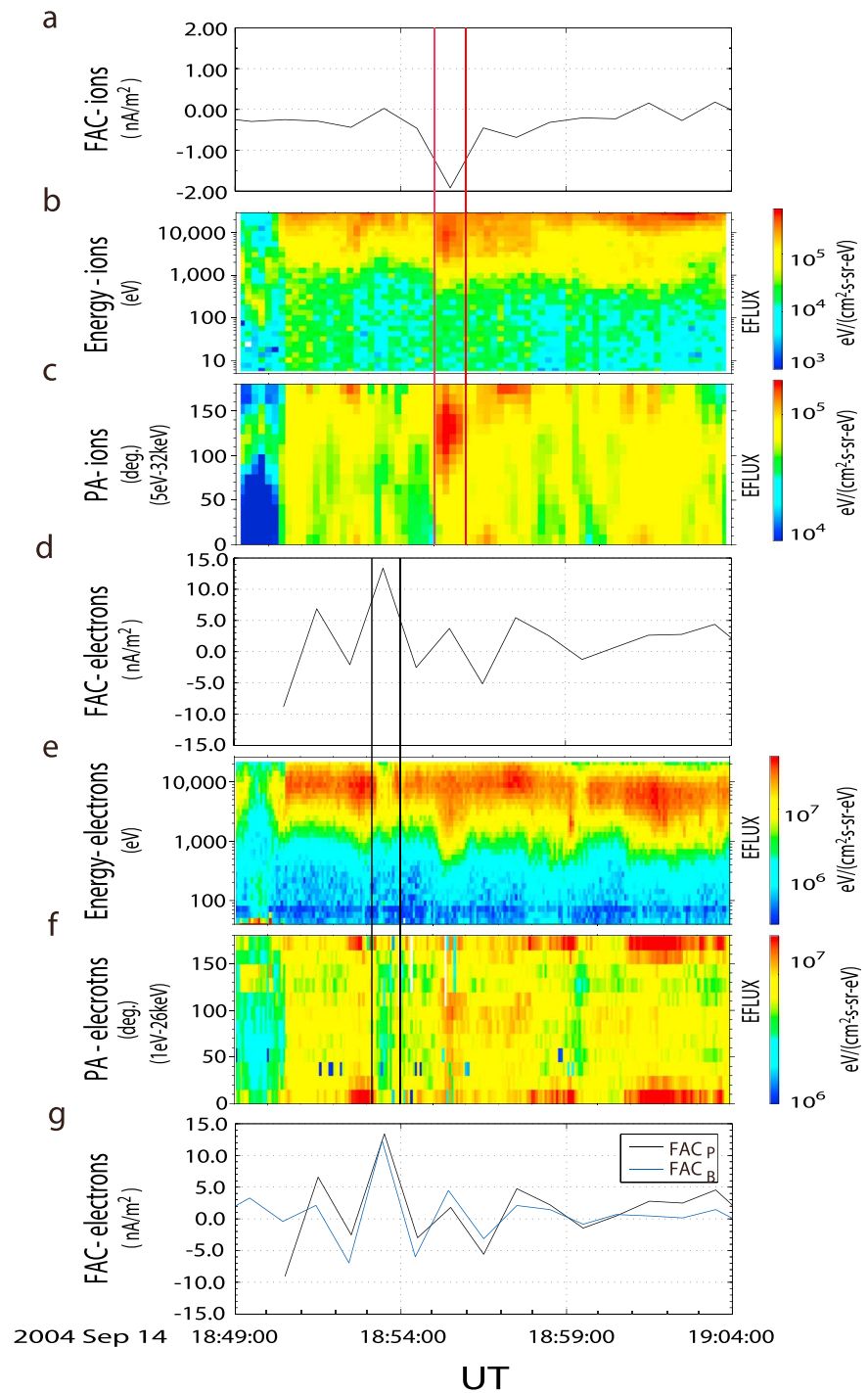


**Figure 3.** In situ HIA/PEACE/FGM measurements of C3 between 1849 to 1904 UT on 14 September 2004. (a) The FACs carried by ions. (b) Ion energy versus time flux spectrogram in the energy range of 5 eV–32 keV. (c) Ion pitch angle (PA) versus time flux spectrogram in the energy range of 5 eV–32 keV. (d) The FACs carried by electrons. (e) Electron energy versus time flux spectrogram in the energy range of 1 eV–26 keV. (f) Electron pitch angle (PA) versus time flux spectrogram in the energy range of 1 eV–26 keV. (g) The densities of FACs were calculated by the two methods (The black line is FAC<sub>P</sub>, which denotes the FAC density calculated with C3 plasma data (ions and electrons). The blue line is FAC<sub>B</sub>, which denotes the FAC density calculated with the magnetic field data.). The large tailward ion FAC density and its corresponding energy range and pitch angle are marked by the two red lines. The large Earthward electron FAC density and its corresponding energy range and pitch angle are marked by the two black lines. The color bar denotes the energy flux (eflux). Note that the color scale panels are in the different ranges.



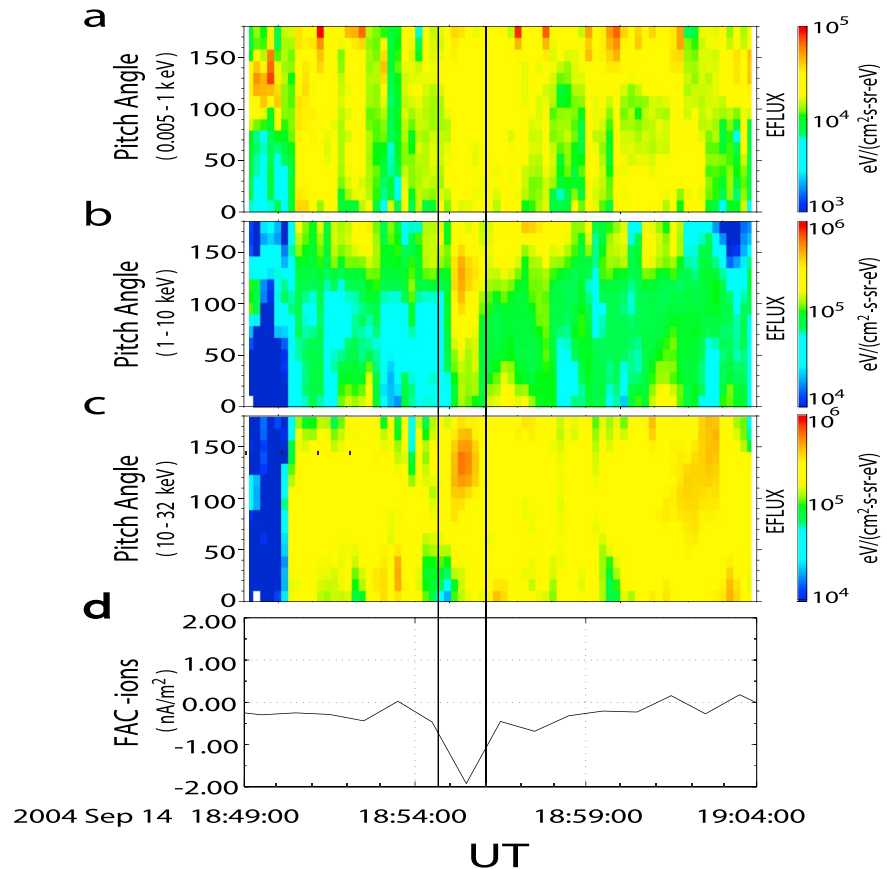


**Figure 4.** Ion pitch angle versus time flux spectrogram in the different energy ranges. (a) Pitch angle versus time flux spectrogram in the energy range of 0.005–1 keV. (b) Pitch angle versus time flux spectrogram in the energy range of 1–10 keV. (c) Pitch angle versus time flux spectrogram in the energy range of 10–32 keV. (d) The FACs which are carried by ions. The large tailward ions FAC density and its corresponding pitch angle spectrogram in different energy ranges are marked by the two vertical black lines. The color bar denotes the energy flux. Note that the color scale in Figure 4a is different from Figures 4b and 4c by a factor of 10.

the CODIF instrument (not shown) and found that the contribution of  $H^+$  is dominant. For electrons, the results are shown in Figure 5. From top to bottom are the pitch angle versus time flux spectrogram in the energy ranges of 0.001 to 0.5, 0.5 to 1, 1 to 10, 10 to 26 keV; the FACs carried by electrons; and the eflux versus pitch angle at the peak and two valleys (Figures 5a–5f). The large earthward FACs and their corresponding energy ranges are marked by the two vertical black lines. The electron fluxes increased obviously above 500 eV (Figures 5b–5d), in roughly the same time period (18:52–18:54 UT) as that of the FAC enhancement. At this point, the electrons (with a density of  $0.25 \text{ cm}^{-3}$ ) carrying the largest FAC have a high bulk speed (more than 500 km/s). The result indicates that FACs were carried by high-speed electrons in the energy range of 0.5 to 26 keV. Figure 5f shows the electron FAC was positive (negative) when the antiparallel (parallel) direction was dominated. We checked all other FAC peaks and found that the FACs were in the antiparallel direction. For all FAC valleys, the currents have parallel directions.

#### 4. Discussion

Most of the time the FAC density calculated with the plasma data is very different to that with magnetic field data. One reason is that the error of the plasma method is often large because the measurements do not include all ions in the full energy range [Frank, 1981; Asano et al., 2004]. Another reason is that the plasma data are locally measured, but the curlometer method calculates the current at the center of the spacecraft tetrahedron contributed by the currents in different locations [Marchaudon et al., 2009]. Therefore, having comparable FAC results from the two methods, as the case presented in the present study, is rare. The FAC

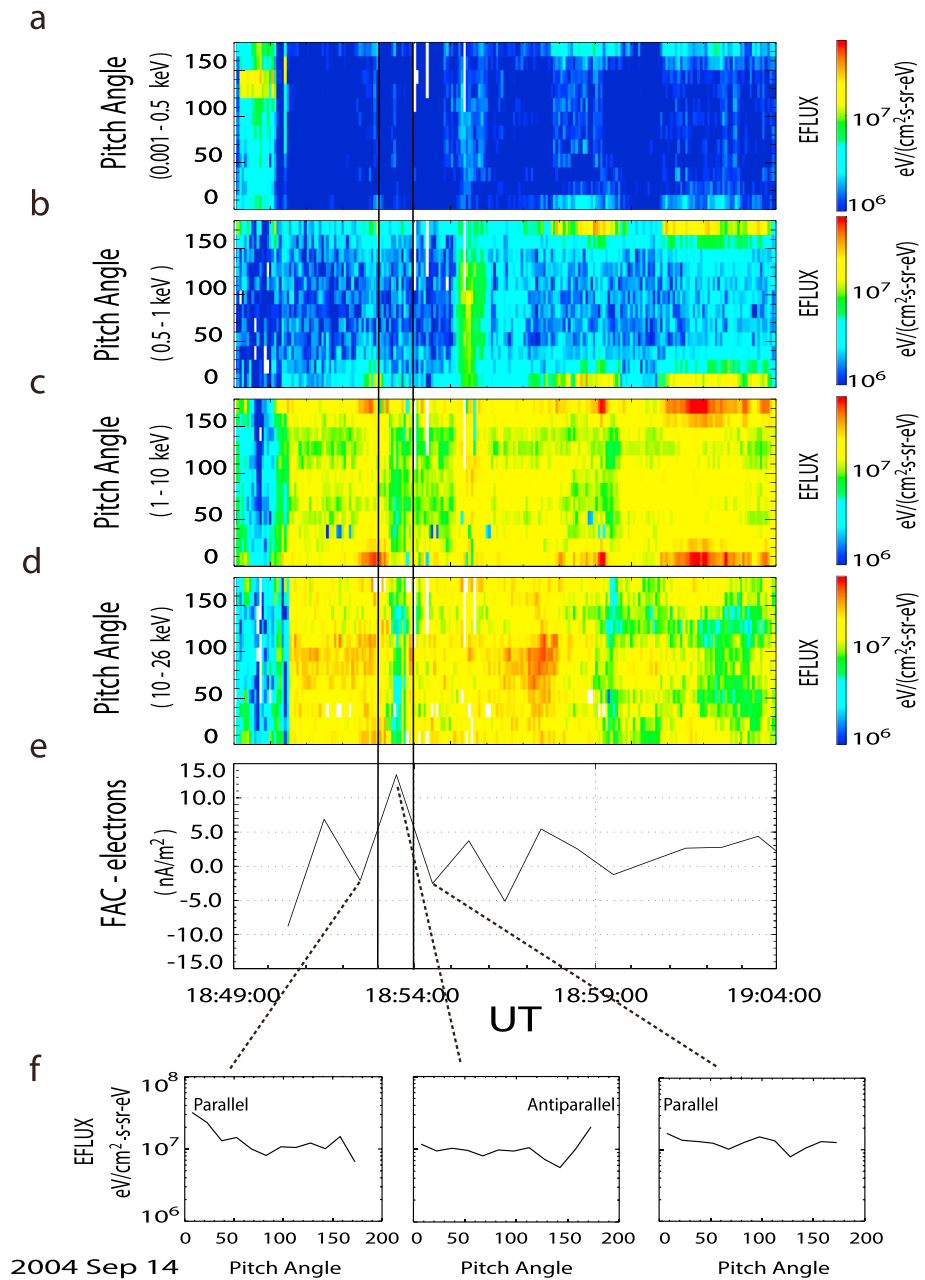


**Figure 5.** Electron pitch angle-time flux spectrograms in the different energy ranges. (a) Pitch angle versus time flux spectrogram in the energy range of 0.001–0.5 keV. (b) Pitch angle versus time flux spectrogram in the energy range of 0.5–1 keV. (c) Pitch angle versus time flux spectrogram in the energy range of 1–10 keV. (d) Pitch angle versus time flux spectrogram in the energy range of 10–32 keV. (e) The FACs carried by electrons. The large Earthward FAC and its corresponding pitch angle spectra in different energy range are marked by the two vertical black lines. (f) The energy flux versus pitch angle at the peak and two valleys. The color bar denotes the energy flux.

densities in the magnetotail are often very small, but during substorms the FAC densities increase rapidly and have larger magnitudes than usual. As a result, it is more likely to investigate the FAC carriers in substorms.

Our results show that during the substorm recovery phase, part of the tailward FACs is carried by energetic antiparallel ions, which are probably originated from the ionosphere through outflow. *Keiling et al.* [2006] identified the ion outflow in the southern PSBL at  $\sim 4.5 R_E$  by the energies and pitch angle ranges of ions (The ion outflow contained both  $H^+$  and  $O^+$ . Energies and pitch angle ranges for  $H^+$  are 10–800 eV and  $< 90^\circ$ , respectively.  $O^+$ , on the other hand, has the same pitch angle range but is less energetic than  $H^+$ ). In



this study, the value of the outward velocity (density) of 78 km/s ( $0.68 \text{ cm}^{-3}$ ) shows that there is strong outflowing plasma. The ions flux has been mapped to 400 and 6000 km, and they are about  $5 \times 10^8$  and  $3 \times 10^7 \text{ cm}^{-2}\text{s}^{-1}$ . They are consistent with the results at low altitudes [Ogawa *et al.*, 2010; Zheng *et al.*, 2005]. The temporal and spatial scale characteristics of ion outflows in the PSBL region at  $\sim 16.4 R_E$  are similar to observations reported by Keiling *et al.* [2006]. The only difference is that the ion outflows in the northern inner PSBL (closer to plasma sheet) are more energetic (more than 1 keV) and the pitch angle range of  $> 90^\circ$  is significantly wider compared to the center plasma sheet ions. This indicates that the high-energy portions of ion distributions are enhanced. The ion outflow in the PSBL contains both  $\text{H}^+$  and  $\text{O}^+$ . We also calculated the FAC densities carried by  $\text{H}^+$  and  $\text{O}^+$  and found that the contribution of  $\text{H}^+$  is dominant. The ion-carried FACs are about  $2 \text{ nA/m}^2$  and thus not too small to be ignored. Thirty-two keV is the upper limit of the HIA instrument. In this study, the energy range of HIA ion measurements does not include the full energy range of the ion carriers. We also checked the Research with Adaptive Particle Imaging Detectors (RAPID) data for higher-energy ions (above 32 keV). Since the fluxes of this part of ion distributions are low, its contribution to FACs is small. Besides, in many cases, the observation of ion flows in the region of FACs does not necessarily mean that these ions are “the carriers” of the FACs but they could be just the flows of charged particles (ions and electrons), appearing in the region of the FACs. As a result, it is important in this study to calculate and compare the FAC densities using both the plasma method and the curlometer method.

The results from our study also show that the earthward FACs are mainly carried by the dominant tailward motion of electrons with large field-aligned bulk speed. That is, electrons are accelerated more easily than ions because the mobility of electrons is higher than that of ions. In the different regions of the geospace, the particle acceleration mechanisms may be different. In the auroral region, the acceleration mechanisms include the parallel electric fields [Alfvén, 1958], Alfvén waves [Hasegawa, 1976], lower hybrid electrostatic turbulence [Bryant, 1994], etc. It is also evident that Alfvén waves also accelerate electrons above the auroral acceleration region along magnetic field lines. For instance, Wygant *et al.* [2002] found accelerated field-aligned electrons in the PSBL, sometimes counter streaming, in the presence of short-perpendicular wavelength Alfvén waves. This indicates that Alfvén waves may have a direct effect on particle acceleration. Keiling *et al.* [2005] also found that Alfvén waves were superimposed on the signature of an FAC in the tail lobe and PSBL regions, especially in substorms. In our study, the FAC of electrons was followed by an FAC in the opposite direction (i.e., the density disturbance appears as peaks and valleys). It implies that the FAC of electrons intermixed with low-frequency waves (with a frequency of about 0.01 Hz) excited by energetic particles. On the other hand, our study also shows that the FAC of ions has only one valley. The pitch angles of electrons are distributed mainly in the parallel and antiparallel directions, but ions are mainly in the antiparallel direction. These ions, probably originated from the ionosphere through outflow, tend to keep their original flow directions along the field lines in the magnetotail. The electrons carry intense FACs whose origin is often related to a general generator region located some distance away [Wright *et al.*, 2002]. In this study, the local electrons in the magnetotail were accelerated and became the main carriers, while obvious fluctuations of FACs were detected. We checked the pitch angles in different energy ranges of electrons and found that higher-energy electrons (from  $\sim 0.5$  to 26 keV) carried the FACs. Twenty-six keV is the upper limit of the PEACE instrument. The energy range of the PEACE measurements includes almost the full energy range of the electron carriers. We also checked the RAPID data for higher energy (above 26 keV). There are signs that some electrons have been accelerated from lower to higher energy, but their contributions to FACs are small.

## 5. Conclusion and Outlook

In conclusion, this study provided a method to study the FAC carriers in the magnetotail in a feasible way by using magnetic field and plasma measurements from multiinstruments, i.e., FGM, PEACE, and CIS, on board the four Cluster spacecraft. From July to October of 2004, in total, each Cluster spacecraft had 63 PSBL crossings during the Cluster tail season. However, only one case, in which FAC results from the plasma method had a good agreement with those from the curlometer method, is found for the present study. It is shown that not only electrons but also ions can carry the FACs in the PSBL. The energy of the ion carriers is  $> 1$  keV, and the energy of the electron carriers is from  $\sim 0.5$  to 26 keV. FAC carriers in the magnetotail are important for the understanding of the energy transfer between the magnetosphere and ionosphere. However, studies on the research topic are rare, because the identification of the exact current carriers is possible only if FAC calculations with the two methods agree with each other. Although we reported one

single case in the present study, the results help advance our understanding of the characteristics of FAC carriers in the magnetotail, especially in the substorm. Four Magnetospheric Multiscale (MMS) spacecraft, similar to the Cluster constellation, were launched recently. Magnetic field and plasma measurements from MMS can be utilized in a similar way for future investigation into the FACs and their particle carriers.

#### Acknowledgments

This work was supported by Natural Science Foundation of China under grants 41374169, 41474137, and 41274146 and the Specialized Research Fund for State Key Laboratories. IMF data and AE/AU/AL were obtained from the GSFC/SPDF OMNIWeb interface at <http://omniweb.gsfc.nasa.gov>. The authors thank the International Space Science Institute in Bern, Switzerland, for supporting the 'Field-Aligned Currents: Their Morphology, Evolution, Source Regions and Generators' international team, from which this work was developed. The authors thank the Cluster team for their data and software. Z. W. Cheng also thanks S. Wang, C. G. Mouikis, and E. Lund for their help and discussion.

#### References

- Alfvén, H. (1958), On the theory of magnetic storms and aurorae, *Tellus*, *10*, 104–116.
- Asano, Y., T. Mukai, M. Hoshino, Y. Saito, H. Hayakawa, and T. Nagai (2004), Current sheet structure around the near-Earth neutral line observed by Geotail, *J. Geophys. Res.*, *109*, A02212, doi:10.1029/2003JA010114.
- Aubry, M. P., M. G. Kivelson, R. L. McPherron, C. T. Russell, and D. S. Colburn (1972), Outer magnetosphere near midnight at quiet and disturbed times, *J. Geophys. Res.*, *77*, 5487–5502, doi:10.1029/JA077i028p05487.
- Balogh, A., et al. (1997), The Cluster magnetic field investigation, *Space Sci. Rev.*, *79*, 65–91.
- Berko, F. W., R. A. Hoffman, R. K. Burton, and R. E. Holzer (1975), Simultaneous particle and field observations of field-aligned currents, *J. Geophys. Res.*, *80*, 37–46, doi:10.1029/JA080i001p00037.
- Bryant, D. A. (1994), Electron acceleration in the aurora, *Contemp. Phys.*, *35*, 165–179.
- Cassery, R. T., and P. A. Cloutier (1975), Rocket-based magnetic observations of auroral Birkeland currents in association with a structured auroral arc, *J. Geophys. Res.*, *80*, 2165–2168, doi:10.1029/JA080i016p02165.
- Chanteur, G. (1998), Spatial interpolation for four spacecraft: Theory, in *Analysis Methods for Multispacecraft Data, ISSI Sci. Rep. SR-001*, 271 pp., Kluwer Acad., Norwell, Mass.
- Cheng, Z. W., J.-K. Shi, T.-L. Zhang, and Z.-X. Liu (2007), Probability of field-aligned currents observed by the satellite Cluster in the magnetotail, *Chin. Phys. Lett.*, *24*(4), 1125–1127.
- Cheng, Z. W., J. K. Shi, M. Dunlop, and Z. X. Liu (2013), Influences of the interplanetary magnetic field clock angle and cone angle on the field-aligned currents in the magnetotail, *Geophys. Res. Lett.*, *40*, 5355–5359, doi:10.1002/2013GL056737.
- Chun, F. K., and C. T. Russell (1991), The evolution of field-aligned currents as a function of substorm phase, *J. Geophys. Res.*, *96*, 15,801–15,810, doi:10.1029/91JA01018.
- Cummings, W. D., and A. J. Dessler (1967), Field-aligned currents in the magnetosphere, *J. Geophys. Res.*, *72*, 1007–1013, doi:10.1029/JZ072i003p01007.
- Dunlop, M. W., D. J. Southwood, K.-H. Glassmeier, and F. M. Neubauer (1988), Analysis of multipoint magnetometer data, *Adv. Space Res.*, *8*(9), 273, doi:10.1016/0273-1177(88)90141-X.
- Dunlop, M. W., A. Balogh, K.-H. Glassmeier, and P. Robert (2002), Four-point Cluster application of magnetic field analysis tools: The curlometer, *J. Geophys. Res.*, *107*(A11), 1384, doi:10.1029/2001JA005088.
- Eastman, T. E., L. A. Frank, and C. Y. Huang (1985), The boundary layers as the primary transport regions of the Earth's magnetotail, *J. Geophys. Res.*, *90*, 9541–9560, doi:10.1029/JA090iA10p09541.
- Eriksson, S., J. W. Bonnell, L. G. Blomberg, R. E. Ergun, G. T. Marklund, and C. W. Carlson (2002), Lobe cell convection and field-aligned currents poleward of the region 1 current system, *J. Geophys. Res.*, *107*(A8), 1185, doi:10.1029/2001JA005041.
- Frank, L. A., L. McPherron, R. J. DeCoster, B. G. Burek, K. L. Ackerson, and C. T. Russell (1981), Field-aligned currents in the Earth's magnetotail, *J. Geophys. Res.*, *86*, 687–700, doi:10.1029/JA086iA02p00687.
- Gombosi, T. I., and A. F. Nagy (1989), Time-dependent modeling of field-aligned current-generated ion transients in the polar wind, *J. Geophys. Res.*, *94*, 359–369, doi:10.1029/JA094iA01p00359.
- Hasegawa, A. (1976), Particle acceleration by MHD surface waves and formation of the aurora, *J. Geophys. Res.*, *81*, 5083–5090, doi:10.1029/JA081i028p05083.
- Iijima, T., and T. A. Potemra (1976), The amplitude distribution of field-aligned currents at northern high latitudes observed by Triad, *J. Geophys. Res.*, *81*, 2165–2174, doi:10.1029/JA081i013p02165.
- Iijima, T., and T. A. Potemra (1978), Large-scale characteristics of field-aligned currents associated with substorms, *J. Geophys. Res.*, *83*, 599–615, doi:10.1029/JA083iA02p00599.
- Johnstone, A. D., et al. (1997), Peace: A plasma electron and current experiment, *Space Sci. Rev.*, *79*, 351–398.
- Keiling, A., G. K. Parks, J. R. Wygant, J. Dombeck, F. S. Mozer, C. T. Russell, A. V. Streltsov, and W. Lotko (2005), Some properties of Alfvén waves: Observations in the tail lobes and the plasma sheet boundary layer, *J. Geophys. Res.*, *110*, A10S11, doi:10.1029/2004JA010907.
- Keiling, A., et al. (2006), Energy-dispersed ions in the plasma sheet boundary layer and associated phenomena: Ion heating, electron acceleration, Alfvén waves, broadband waves, perpendicular electric field spikes, and auroral emissions, *Ann. Geophys.*, *24*, 2685–2707, doi:10.5194/angeo-24-2685-2006.
- Marchaudon, A., J.-C. Cerisier, M. W. Dunlop, F. Pitout, J.-M. Bosqued, and A. N. Fazakerley (2009), Shape, size, velocity and field-aligned currents of dayside plasma injections: A multi-altitude study, *Ann. Geophys.*, *27*, 1251–1266, doi:10.5194/angeo-27-1251-2009.
- McDiarmid, I. B., J. R. Burrows, and M. D. Wilson (1978), Comparison of magnetic field perturbations at high latitudes with charged particle and IMF measurements, *J. Geophys. Res.*, *83*, 681–688, doi:10.1029/JA083iA02p00681.
- Möbius, E., et al. (1998), The 3-D plasma distribution function analyzers with time-of-flight mass discrimination for CLUSTER, FAST, and Equator-S, in *Measurement Techniques in Space Plasmas: Particles*, edited by R. F. Pfaff et al., pp. 243–248, AGU, Washington, D. C.
- Moore, T. E., M.-C. Fok, and K. Garcia-Sage (2014), The ionospheric outflow feedback loop, *J. Atmos. Sol. Terr. Phys.*, *113–114*, 59–66, doi:10.1016/j.jastp.2014.02.002.
- Morooka, M., T. Yamamoto, T. Mukai, K. Tsuruda, H. Hayakawa, and H. Fukunishi (1998), Relationship between field-aligned currents and parallel electric field observed by Akebono, in *Substorms-4*, edited by S. Ko-kubun and Y. Kamide, pp. 59–62, Kluwer Acad., Norwell, Mass.
- Ogawa, Y., S. C. Buchert, A. Sakurai, S. Nozawa, and R. Fujii (2010), Solar activity dependence of ion upflow in the polar ionosphere observed with the European Incoherent Scatter (EISCAT) Tromsø UHF radar, *J. Geophys. Res.*, *115*, A07310, doi:10.1029/2009JA014766.
- Ohtani, S., S. Kokubun, R. C. Elphic, and C. T. Russell (1988), Field-aligned current signatures in the near-tail region: 1. ISEE observations in the plasma sheet boundary layer, *J. Geophys. Res.*, *93*, 9709–9720, doi:10.1029/JA093iA09p09709.
- Rème, H., et al. (2001), First multispacecraft ion measurements in and near the Earth's magnetosphere with the identical Cluster ion spectrometry (CIS) experiment, *Ann. Geophys.*, *19*, 1303–1354, doi:10.5194/angeo-19-1303-2001.
- Shi, J. K., et al. (2010), South-north asymmetry of field-aligned currents in the magnetotail observed by Cluster, *J. Geophys. Res.*, *115*, A07228, doi:10.1029/2009JA014446.

- Shi, J. K., Z. Zhang, K. Torkar, M. Dunlop, A. Fazakerley, Z. Cheng, and Z. Liu (2014), Temporal and spatial scales of a high-flux electron disturbance in the cusp region: Cluster observations, *J. Geophys. Res. Space Physics*, *119*, 4536–4543, doi:10.1002/2013JA019560.
- Strangeway, R. J., C. T. Russell, C. W. Carlson, J. P. McFadden, R. E. Ergun, M. Temerin, D. M. Klumpar, W. K. Peterson, and T. E. Moore (2000), Cusp field-aligned currents and ion outflows, *J. Geophys. Res.*, *105*, 21,129–21,141, doi:10.1029/2000JA900032.
- Torbert, R. B., and C. W. Carlson (1980), Evidence for parallel electric field particle acceleration in the dayside auroral oval, *J. Geophys. Res.*, *85*, 2909–2914, doi:10.1029/JA085iA06p02909.
- Ueno, G., S. Ohtani, Y. Saito, and T. Mukai (2002), Field-aligned currents in the outermost plasma sheet boundary layer with Geotail observation, *J. Geophys. Res.*, *107*(A11), 1399, doi:10.1029/2002JA009367.
- Welling, D. T., V. K. Jordanova, A. Glocer, G. Toth, M. W. Liemohn, and D. R. Weimer (2015), The two-way relationship between ionospheric outflow and the ring current, *J. Geophys. Res. Space Physics*, *120*, 4338–4353, doi:10.1002/2015JA021231.
- Winglee, R. M., W. Lewis, and G. Lu (2005), Mapping of the heavy ion outflows as seen by IMAGE and multifluid global modeling for the 17 April 2002 storm, *J. Geophys. Res.*, *110*, A12S24, doi:10.1029/2004JA010909.
- Wright, A. N., W. Allan, M. S. Ruderman, and R. C. Elphic (2002), The dynamics of current carriers in standing Alfvén waves: Parallel electric fields in the auroral acceleration region, *J. Geophys. Res.*, *107*(A7), 1120, doi:10.1029/2001JA900168.
- Wright, A. N., C. J. Owen, C. C. Chaston, and M. W. Dunlop (2008), Downward current electron beam observed by Cluster and FAST, *J. Geophys. Res.*, *113*, A06202, doi:10.1029/2007JA012643.
- Wygant, J. R., et al. (2002), Evidence for kinetic Alfvén waves and parallel electron energization at 4–6  $R_E$  altitudes in the plasma sheet boundary layer, *J. Geophys. Res.*, *107*(A8), 1201, doi:10.1029/2001JA900113.
- Yamauchi, M., R. Lundin, L. Eliasson, S. Ohtani, and J. H. Clemmons (1998), Relationship between large-, meso-, and small-scale field-aligned currents and their current carriers, in *Polar Cap Phenomena*, pp. 173–188, Kluwer Acad, Norwell, Mass.
- Zhang, L. Q., Z. X. Liu, Z. W. Ma, C. Shen, X. Z. Zhou, and X. G. Zhang (2007), Effect of upward ion on field-aligned currents in the near-Earth magnetotail, *Sci. China, Ser. G: Phys., Mech. Astron.*, *50*(5), 673–680.
- Zheng, Y., T. E. Moore, F. S. Mozer, C. T. Russell, and R. J. Strangeway (2005), Polar study of ionospheric ion outflow versus energy input, *J. Geophys. Res.*, *110*, A07210, doi:10.1029/2004JA010995.
- Zmuda, A. J., J. H. Martin, and F. T. Heuring (1966), Transverse magnetic disturbances at 1100 kilometers in the auroral region, *J. Geophys. Res.*, *66*, 5033–5045, doi:10.1029/JZ071i021p05033.